Imaging Arithmetic: Physics ∪ Math > Physics + Math

Gaurav Sharma

Electrical and Computer Engineering and Biostatistics & Computational Biology Depts.
RC Box 270126, University of Rochester, Rochester, NY 14627-0126

ABSTRACT

Imaging devices operate at the physical interfaces corresponding to image capture and reproduction. The combination of physical insight and mathematical signal processing tools, therefore, offers unique advantages in solving problems in imaging systems. In this paper, we illustrate and support this idea using examples from our research on imaging, where the combination of physical insight, mathematical tools, and engineering ingenuity leads to elegant and effective solutions.

Keywords: Imaging Systems, Physical Imaging, Modeling

1. INTRODUCTION

The theory of signal and image processing is rooted in a strong mathematical foundation. This is evident from fundamental texts on these topics [1–3] that present signal and image processing concepts in an elegant and typically abstract mathematical framework. This approach has the benefit of unifying the presentation of key concepts and encompassing a wide range of different cases within the analysis, and has demonstrated significant success in practice. A prime example of the approach is the ubiquitous use of frequency representations based on Fourier theory which significantly simplifies the analysis of linear time/shift invariant systems. Additional examples that we build on in the course of this paper are linear algebra that leads to useful signal space representations, first developed in the context of communication systems [4], and set theoretic estimation methods for signal estimation and recovery [5].

For several real-world problems, signal and image processing approaches are most successful when they combine the insight offered by the physics of the problem with the mathematical framework and tools inherent in digital signal processing. To quote Simon Haykin [6]:

"Signal processing is at its best when it successfully combines the unique ability of mathematics to generalize with both the insight and prior information gained from the underlying physics of the problem at hand."

Imaging systems are a particularly fertile ground for problems in this class because they deal specifically with the capture of physical scenes and with the reproduction of images on physical devices. Physical interactions are thus at the heart of most imaging problems. Solutions for these problems that combine physical understanding and modeling with appropriate mathematical tools of signal/image processing, offer in the combination, advantages significantly greater than would be estimated as the sum of the individual parts*. In this paper, we highlight specific examples† of problems in physical imaging for which the happy marriage between physical insight and modeling and appropriate mathematical methods leads to novel solutions. Two case studies are presented in some detail and additional examples are briefly summarized.

The rest of this paper is organized as follows. In section 2, we highlight the phenomenon of show-through in document imaging and illustrate how the combination of simple physical modeling with the powerful signal processing technique of adaptive filtering leads to an effective method for correction of show-through in scanned

Further author information: (Send correspondence to Gaurav Sharma.)
E-mail: gaurav.sharma@rochester.edu, Telephone: 1 585 275 7313

*Hence the title for this paper.

†The examples in the paper are derived from my own work, even though there are numerous other and significantly better examples of work by others in the same vein. I apologize for the biased sampling. The only justification I can offer is that I have access to and am most familiar with my own work.

Color Imaging X: Processing, Hardcopy, and Applications, edited by Reiner Eschbach, Gabriel G. Marcu,
Proc. of SPIE-IS&T Electronic Imaging, SPIE Vol. 5667 © 2005 SPIE and IS&T · 0277-786X/05/$15

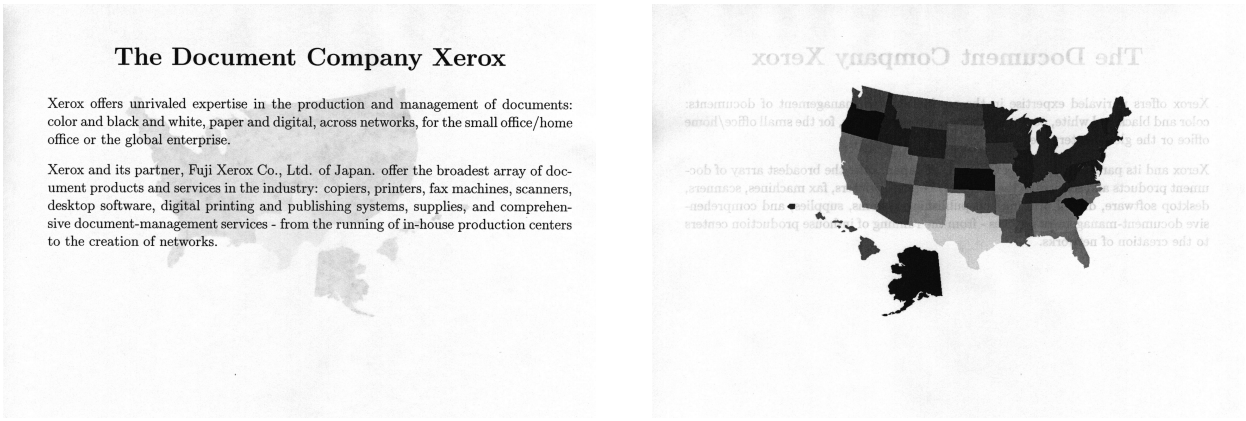

(a) Side 1 (b) Side 2

Figure 1. Scans of two sides of a duplex printed page. (From [7])

documents. Next in section 3, we show how the blend of physical modeling with the mathematical tools of linear algebra and set-theoretic estimation leads to useful solutions to problems in subtractive color systems. Finally in section 4, we present a discussion and summary along with references to additional examples of research that support the inequality in our title. Note that the research for the two individual cases covered here has previously been published in more detailed individual contributions on show-through correction [7] and set-theoretic estimation for subtractive color [8, 9].

2. SHOW-THROUGH IN DOCUMENT IMAGING

Duplex or double-sided printing is commonly used for hardcopy documents, with most magazine and book pages being prime examples. When a duplex printed page is scanned, information from the back-side printing can often be seen in the scan (of the front side of the page). This show-through is normally an undesirable artifact in the scanned images that one would like to remove. An example of show-through can be seen in Fig. 1 where the scans from two sides of a duplex printed page are shown. Show-through from the back side can clearly be seen in either scan [‡]. From the figure, one can also note that, the dynamic range (i.e., contrast) of the show-through information is typically much lower than the dynamic range of the printing on the front side. This is a manifestation of the physical fact that the transmittance of paper is low (in relation to its reflectance).

Traditionally thresholding is used to minimize the effect of show-through. Thresholding sets scanned reflectance values above a selected threshold to unity (white). This approach works well for pure black and white regions (e.g. Fig. 1 (a)), but fails irretrievably for show-through seen in a light gray background, for instance, in the region corresponding to the state of Texas in Fig. 1 (b).

Without additional information, one cannot distinguish low contrast information due to light gray printing in the front side from show-through and it is difficult to improve on the thresholding solution. However, when scans from both sides of the document are available (for instance in automatic feed duplex scanners) one can use the scan from the back-side to distinguish these two cases. However, in order to remove show-through from the light gray regions such as the region corresponding to the state of Texas in Fig. 1 (b), not only must one identify regions with show-through but it is also necessary to determine the contribution of show-through. A physical model of the scanning process is required for this purpose, which we develop next.

[‡]In order to ensure that information in the light document regions (in which show-through effects are seen) are not lost due to truncation in the uncalibrated system through which this paper is reproduced, all images reproduced here have been mapped through a *single* tone-adjustment curve that emphasizes the detail in this region. Images may, however, still not reproduce well in print.

2.1. Physical Model for Show-through

The image captured by a scanner is a two dimensional array of pixels, where each pixel value represents the reflectance of the document at the physical location corresponding to that pixel. The most common type of scanner is a flat-bed scanner. Fig. 2 (a) shows a schematic of the optical components of a flat-bed scanner. The document to be scanned is laid face down on a transparent glass platen and pressed flat against the platen by a backing. The scanner lamp illuminates the document through the platen glass and the light reflected off the spatial location corresponding to a given pixel is imaged by a lens onto a sensor. The resulting signal is digitized to obtain a representation of the image as a reflectance profile. Typically, the sensors are laid out in a linear CCD array, which allows for an entire row of pixels along one dimension of the document to be imaged in a single exposure step. The array is moved across the document and multiple exposures are performed to capture the complete two-dimensional image.

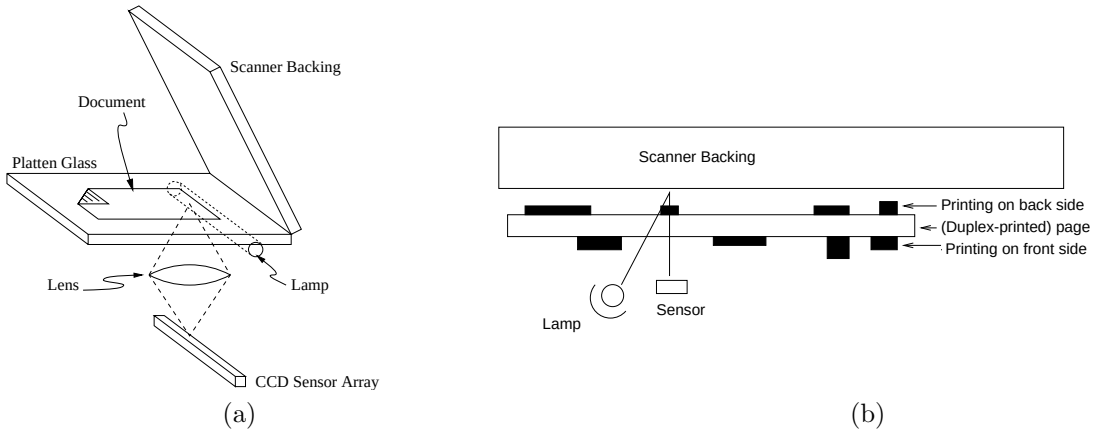

Figure 2. Scanner model: (a) Optical schematic, (b) Duplex page scan.

Fig 2 (b) illustrates the process of scanning one side of a duplex printed page on a typical scanner, where the arrangement of the duplex printed page of paper in relation to scanner lamp, sensor, and backing is shown in a cross-sectional view. The process can be analyzed using a simplified physical model that comprehends the relevant properties of the document and the scanner. The paper can be characterized in terms of the fraction of light S_p that it scatters (reflects) back and the fraction T_b that it transmits. The printed information on each side can be modeled in terms of the spatial transmittance profiles, $T_f(x, y)$ and $T_b(x, y)$, of the "printing layers" on the front and back sides, respectively. The light reaching the sensor at the spatial location (x, y) has two main components: a) light that encounters the front side printing layer is reflected from the paper substrate and encounters the front-side printing layer again, this corresponds to a fraction $T_f^2(x, y)S_p$ of the incident light and b) light that goes through the front printing layer, the paper, and the back printing layer; is reflected by the scanner backing; and encounters the three layers again on its return path; this corresponds to a fraction $T_f^2(x, y)T_b^2(x, y)T_pR_{bk}$ of the incident light, where R_{bk} is the reflectance of the scanner backing. Thus, the reflectance detected by the sensor when scanning the front side is given by the sum of these two fractions as

$$R_f^s(x, y) = T_f^2(x, y)(S_p + T_p^2 R_{bk} T_b^2(x, y)) \tag{1}$$

where the subscript f denotes the front side, and the superscript s is used to denote that this is the "scanned" reflectance.

Equation (1) indicates that the reflectance $R_f^s(x, y)$ detected by the scanner sensor depends on the front-side print layer transmittance, the paper scattering and transmittance parameters, the reflectance of the backing, and the back-side print layer transmittance. In particular, the dependence of the scanned reflectance $R_f^s(x, y)$ for the front side on the transmittance $T_b(x, y)$ of the back side print layer represents the undesired show-through in the front side scan. The equation also suggests a direct physical method for the elimination of show-through by

setting $R_{bk} = 0$, i.e., using a black backing. This solution however produces undesirable black output for holes and uncovered margin regions in the document and also encounters higher noise due to the variability in paper transmittance, making alternate electronic methods for the correction of show-through more desirable.

2.2. Show-through Analysis and Correction

The goal of show-through correction is to recover the "image" $T_f(x, y)$ printed on the front side with no dependence on the back side "image" $T_b(x, y)$. Recovery of the show-through corrected image cannot be accurately done using the front-side scan alone because it is not possible to reliably distinguish between light gray printing on the front-side and low-contrast show-through from the back-side. Mathematically, this is manifested in the fact that the single equation (1) cannot be solved simultaneously for the two unknowns, $T_f(x, y)$ and $T_b(x, y)$. If the scan of the back-side is also available, then analogous to (1), the scanned reflectance for the back side can be written as

$$R_b^s(x, y) = T_b^2(x, y)(S_p + T_p^2 R_{bk} T_f^2(x, y)) \tag{2}$$

where the terms on the right hand side are as defined earlier.

Given (1) and (2), we can expect to remove show-through if scans of both sides of the page are available and if these two equations can be solved for the two unknowns, $T_f(x, y)$ and $T_b(x, y)$. In practice, the situation is not so simple because several of the parameters are unknown and (more significantly) the point-wise model of interaction is an oversimplification. To address these hurdles, it is advantageous to first transform the equations from reflectance to normalized optical density[§], as

$$D_f^s(x, y) \equiv -\ln \frac{R_f^s(x, y)}{R_p^w} = D_f(x, y) - \ln\left(1 - \frac{T_p^2 R_{bk}}{S_p + T_p^2 R_{bk}}(1 - T_b^2(x, y))\right) \tag{3}$$

where $R_p^w = S_p + T_p^2 R_{bk}$ is the (scanned) reflectance for "white" paper that has no printing on either side and $D_f(x, y) = -\ln(T_f^2(x, y))$ denotes the normalized front side scan density that would have been obtained in the absence of any printing on the back-side, which we refer to as the *desired* front side scan density.

For typical paper substrates, the fraction of light transmitted is much smaller than the fraction of light scattered, i.e., $T_p^2 << S_p$. This assumption is directly supported by the observation that most paper substrates appear close to white, even when placed on a black backing. This allows us to significantly simplify (3) using the approximation $\ln(1 - t) \approx -t$ for $|t| << 1$, where $t = \frac{T_p^2 R_{bk}}{S_p + T_p^2 R_{bk}}(1 - T_b^2(x, y))$. With this approximation, (3) becomes

$$D_f^s(x, y) \approx D_f(x, y) + \frac{T_p^2 R_{bk}}{S_p + T_p^2 R_{bk}} A_b(x, y) \tag{4}$$

where $A_b(x, y) = (1 - T_b^2(x, y))$ is the "absorptance" of the back side "print layer".

Equation (4) states that the paper-normalized density of the front side scan can be approximated by the sum of the paper-normalized density of the show-through corrected front side and the absorptance of the back-side print layer weighted by a small factor. It is clear that the second term represents the show-through. An equivalent equation is also readily derived for the back-side. The major significance of these equations is that in the density domain the show-through separates into an additive distortion, which is further characterized as being a scalar multiple of the absorptance of the printing layer on the opposite side.

In order to further incorporate the physical effect of the spreading of light in paper into our model, the term $\frac{T_p^2 R_{bk}}{S_p + T_p^2 R_{bk}}$, in (4) may be replaced with with an empirical "show-through" point spread function (PSF) to obtain

$$D_f^s(x, y) \quad = \quad D_f(x, y) + h(x, y) \otimes A_b(x, y), \tag{5}$$

[§]Note that conventionally the logarithm to the base 10 is used in defining density, but for notational simplicity the natural logarithm is used throughout this paper

where $h(x, y)$ is the "show-through point spread function" and $\otimes$ represents the convolution operator. Since show-through PSF is a replacement for the term $\frac{T_p^2 R_{bk}}{S_p + T_p^2 R_{bk}}$ in the physical model, it is clear that $h(x, y)$ is small in comparison to unity and physically accounts for the transmission and spreading of light in the paper and the reflectance of the backing.

In order to "solve" (5) for the desired or show-through corrected front side density $D_f(x, y)$ the absorptance of the back side "image layer" , i.e., $A_b(x, y)$ may further be approximated[¶] using the estimate based on the back side scan $A_b^s(x, y) = (1 - R_b^s(x, y)/R_p^w))$. With this approximation, (5) can be re-written as

$$D_f(x, y) = D_f^s(x, y) - h(x, y) \otimes A_b^s(x, y) \tag{6}$$

Adaptive filtering based Show-through Cancellation

The show-through point-spread function $h(x, y)$ is unknown in (6) and, in practical situations, so is the exact alignment between the front and back side scans. Hence the "solution" above is not directly usable. However, we can note that (6) is an exact 2-D analog of the one dimensional echo cancellation problem in speech telephony [10, pp. 327]. Linear adaptive filtering methods that have been successfully applied to speech echo cancellation are thus equally applicable to the show-through removal/cancellation problem, with suitable modifications for the 2-D signals.

Using adaptive filters, the show-through point-spread function can automatically be estimated and tracked as it undergoes changes due to (smooth) local variations in alignment between the front and back side images. Note that this is feasible only because the physical model and the approximation described earlier make the problem a linear one when the front side image data is in the density domain and the back-side image data is in the absorptance domain.

The adaptive filtering process works as follows. At each pixel location (x, y) corresponding to the front side image, the show-through contribution to the scan density is estimated as a weighted sum of back-side absorptance values from the corresponding region on the back side, $\sum_{(x',y')\in S} w(x', y') A_b^s(x - x', y - y')$, where $w(x', y')$ denote the coefficients of the adaptive filter and S denotes the support of the filter. The corrected front side density $D_f(x, y)$ is then estimated by subtracting this estimated show-through contribution from the front side scan density computed as per (3). The processing is then repeated for the next pixel location, continuing until the complete image has been processed. The filter coefficients $w(x', y')$ themselves are adapted in regions with printing on the back side and no printing on the front side, which can be determined from a comparison of image values over neighborhoods in the two sides. The adaptation of the filter coefficients can be done in accordance with any of the several known algorithms in adaptive filter theory [10]. The simplest method, is the least mean-squared (LMS) adaptation method that corresponds to gradient descent with an instantaneous approximation to the gradient. Details of implementation of show-through cancellation using the LMS algorithm may be found in Ref. 7.

Once the image is processed, estimated values of the show-through corrected or desired front-side scan density may be converted to reflectance or any other suitable representation for the image. Show-through corrected images corresponding to the scans of two sides shown earlier in Fig 1, obtained using the show-through cancellation algorithm developed are shown in Fig. 3. From the results it is clear that the algorithm successfully cancels show-through. It is effective in eliminating not only the show-through in white regions of the page but also in light gray regions, such as the regions corresponding to the state of Texas in these figures.

In order to visualize the show-through PSF, the adaptive filter coefficients $w(x', y')$ were recorded at several positions in the processing of the image-side scan. The filter coefficients at two different image locations are shown in Fig. 4. The filter coefficients have a primarily unimodal distribution, which is consistent with what is expected physically for the show-through PSF.

We demonstrated in this section an effective algorithm for the correction of show-through in duplex printed scans that illustrated the "Physics U Math > Physics + Math" principle alluded to in the title of this paper. In the next section, we consider another example illustrating this "inequality" in the context of subtractive color imaging systems.

[¶]Ref. 7 justifies the use of this approximation through additional analysis.

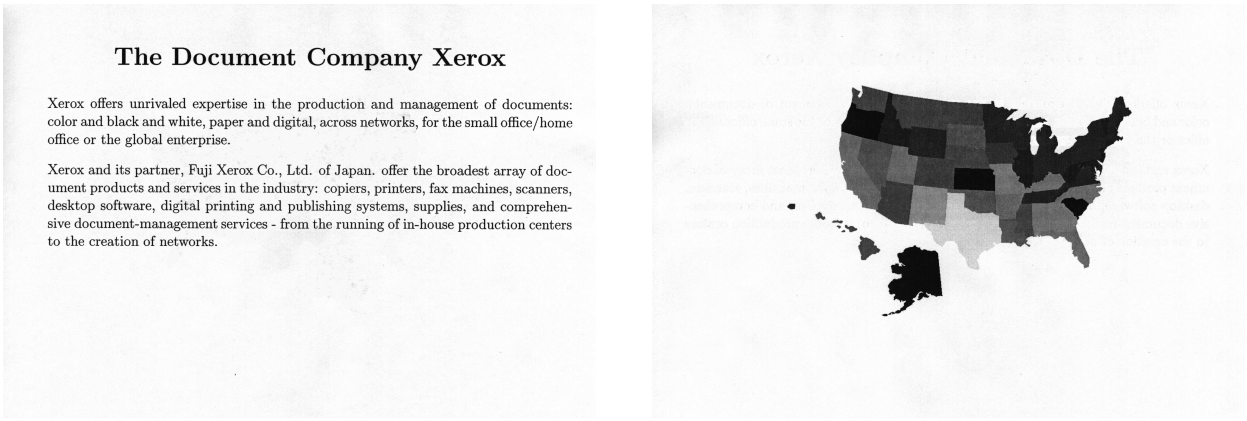

(a) (b)

Figure 3. Scanned data after show-through correction: (a) Side 1 (b) Side 2.

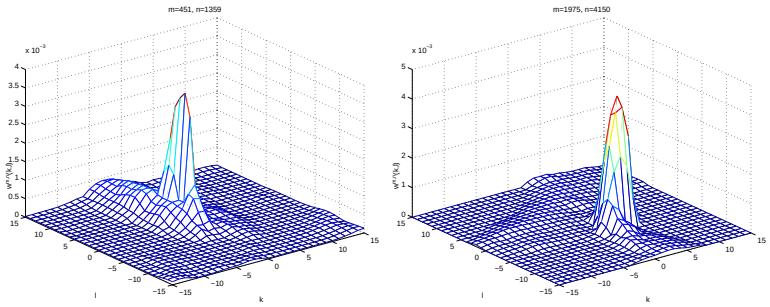

Figure 4. Adaptive filter coefficients $w(x', y')$ at two different image locations.

3. SUBTRACTIVE COLOR SYSTEMS AND SET-THEORETIC ESTIMATION

Physical models for color sensing and additive color systems naturally lend themselves to mathematical modeling in a vector-space framework [11–14]. The power of the vector space approach is further enhanced when it is combined with set theoretic estimation, which has proven a powerful technique for solving signal and image processing problems [5]. The vector space and set theoretic approaches have been combined and successfully applied to several problems in color science and color systems [8, 15, 16]. In this section, we highlight the effectiveness of combining physical modeling with the mathematical method of projections onto convex sets (POCS) for the purpose of solving problems in subtractive color. We restrict our attention here to the application of target-less scanner color calibration [9] additional examples of applications where the same framework is useful may be found in [8].

Typical scanner color calibration is done empirically by scanning a pre-measured calibration target and determining the transformation that maps the scanner RGB values to the measured colorimetric values for the calibration target. The calibration is accurate over the medium represented by the calibration target (i.e., composed of same substrate, same colorants, and same color separation method if there are more than three colorants), but its performance over other media is significantly poorer. In practice, lack of calibration targets for each scanned medium limits the accuracy of the empirical scanner calibration method. At present, scanner calibration targets are available only from a handful of manufacturers of photo-processing products [17]. In addition printed images that are to be scanned, need not correspond to the same type and batch of substrate and colorants that were used in the targets.

Here we present a model-based scanner calibration method, which unlike the empirical calibration, does not require a calibration target. Instead, the method utilizes physical models for the medium and the scanner along

with the mathematical tool of set theoretic estimation [5] to obtain a calibration transformation. First, from direct measurements or indirect estimation methods spectral models are obtained for the scanner and for the medium of interest. The calibration is then performed by determining for each set of scanner RGB values, a feasible reflectance spectrum for the given medium that would give rise to specified RGB values. The calibration process thus defines a transformation from scanner measurements to spectra (on the given medium) that result in those measurements. The spectra can be readily used to obtain color tristimuli under any desired viewing illuminant, which is an additional advantage over schemes that transform scanner measurements into color tristimuli under a particular viewing illuminant.

While useful models are clearly not available for arbitrary media, the Beer-Bouger law and Kubelka-Munk theory provide useful models for photographic transparencies and prints, which fortunately constitute a significant fraction of scanned inputs. In this paper, we present a target-less method for calibration for these media.

3.1. Spectral Model for Photographic Media

Typical photographic transparencies (and slides) are composed of cyan, magenta, and yellow dyes dispersed in a transparent substrate. Different colors required in an image are produced by varying the amounts of the three dyes. The dyes and the substrate have negligible scatter and therefore the spectral transmittance of photographic transparencies is well modeled by the Beer-Bouger law [18, Chap. 7]. Using the Beer-Bouger law, the transmittance of a sample can be computed from the corresponding dye concentrations as

$$t(\lambda) = r_p(\lambda) \exp\left(-\sum_{i=1}^{3} c_i d_i(\lambda)\right) \tag{7}$$

where λ denotes wavelength, $r_p(\lambda)$ is the transmittance of the substrate, $\{c_i\}_{i=1}^3$ are the concentrations, and $\{d_i(\lambda)\}_{i=1}^3$ the spectral densities of the cyan, magenta, and yellow dyes, respectively, corresponding to unity concentrations. An identical mathematical model is applicable for reflective photographic prints with a suitable re-definition of terms [9].

For computational purposes, it is convenient to represent spectra as N-vectors consisting of N uniformly-spaced samples over a suitable wavelength interval that covers the spectral region over which the scanner or the eye are sensitive. Using this sampled representation, (7) becomes

$$\mathbf{r} = \mathbf{r}_p \otimes \exp\left(-\mathbf{D}\mathbf{c}\right) \tag{8}$$

where $\mathbf{r}_p$ is the spectral reflectance of the paper substrate, $\mathbf{D} = [\mathbf{d}_1, \mathbf{d}_2, \mathbf{d}_3]$ is the matrix of colorant densities at unity concentrations, $\mathbf{c}$ is the vector of normalized colorant concentrations corresponding to the reflectance $\mathbf{r}$, $\otimes$ represents the term by term multiplication operator for N-vectors, and the bold lower case terms represent the spectral N-vectors for the corresponding quantities in (7).

The model of (8) provides a means for determining the spectral reflectance of a sample from the concentrations for the cyan, magenta, and yellow dyes. If the range of variation of the concentrations is known, equation (8) can be used to determine the set of all reflectance spectra that are producible on the given medium. For example, if the measured dye densities correspond to the maximum concentrations, the set of reflectance spectra producible on the medium can be expressed as

$$S_0^{med} = \{\mathbf{r} = \mathbf{r}_p \otimes \exp(-\mathbf{D}\mathbf{c}) \;\mid\; \mathbf{c} \in \mathbb{R}^3, 0 \le c_i \le 1\} \tag{9}$$

Since pure cyan, magenta, and yellow tone prints are not normally available in images, the densities corresponding to the dyes cannot be directly measured. Note, however, that by taking the natural logarithm the spectra in the model of (8) can be rewritten in terms of density as

$$\ln(\mathbf{r}_p) - \ln(\mathbf{r}) = \mathbf{D}\mathbf{c} = \sum_{i=1}^{3} c_i \mathbf{d}_i \tag{10}$$

The left-hand side in the above equation represents the density corresponding to the reflectance $\mathbf{r}$ relative to the white paper reflectance $\mathbf{r}_p$. From the above equation, it is clear that these paper-relative spectral densities are linear combinations of the three dye densities $\{\mathbf{d}_i\}_{i=1}^3$. Hence, the paper-relative spectral densities lie in a three dimensional subspace of the overall N-dimensional space containing the spectral density vectors (excluding noise effects). Principal components analysis (PCA) [19] provides a means for determining a set of basis vectors for this three dimensional space.

PCA of an ensemble of paper relative densities computed from a set of representative spectra in accordance with the left hand side of (10) yields three significant principal components that explain almost the entire variation in the data [20]. These three significant principal components, referred to as *principal dye densities* [21], form an orthonormal basis set for the three dimensional space in which paper relative densities lie. Though the principal components do not correspond to actual dye densities, they span the same subspace as the actual dye densities, i.e., any vector that is expressible as a linear combination of three dye densities can also be expressed as a linear combination of the three principal components, and vice versa. Thus, if the actual densities corresponding to the dyes are not known, the principal dye densities determined from PCA can be used in the model of (9) instead of the actual densities [20,21]. While the concentrations corresponding to the real dye densities in (9) were subject to simple upper and lower bounds, similar bounds cannot be obtained for "concentrations" corresponding to the virtual dyes obtained from the principal components analysis. The information in the bounds is therefore lost in this method.

The "principal dye" densities can be determined from a small number of spectral measurements on the scanned images themselves and therefore do not require a calibration target. If $\mathbf{O} = [\mathbf{o}_1, \mathbf{o}_2, \mathbf{o}_3]$ is the matrix of the (orthogonal) principal dye densities (obtained through the principal components analysis), the constraint set

$$S^{med} = \{\mathbf{r} = \mathbf{r}_p \otimes \exp(-\mathbf{O}\mathbf{c}) \;\mid\; \mathbf{c} \in \mathbb{R}^3\} \tag{11}$$

can be used to describe producible spectra on the given medium (strictly speaking, this set is a super-set of the producible spectra).

3.2. Color Scanner Model

For a color scanner, the optical model is the same as that presented in Fig 2, with the single channel sensor replaced by a sensor with three channels with red, green and, blue color filters. For sensors commonly used in electronic scanners, the sensor response is linear and can be modeled as

$$t_i = \int_{-\infty}^{\infty} f_i(\lambda)\, d(\lambda)\, r(\lambda)\, l_s(\lambda)\, d\lambda = \int_{-\infty}^{\infty} m_i(\lambda)\, r(\lambda)\, d\lambda \qquad i = 1, 2, \ldots 3 \tag{12}$$

where t_i represents the scanner response for the i^{th} channel, $\{f_i(\lambda)\}_{i=1}^3$ are the spectral transmittances of the color filters (and other optical components), $d(\lambda)$ is the sensitivity of the detector used in the measurements, $l_s(\lambda)$ is the spectral radiance of the illuminant, $r(\lambda)$ is the spectral reflectance of the pixel being scanned, and $m_i(\lambda) = l_s(\lambda)\, d(\lambda)\, f_i(\lambda)$ is the overall spectral sensitivity of the i^{th} scanner channel that incorporates the illuminant spectral irradiance, the detector sensitivity, and the spectral transmittance of the color filter and other optical components.

Once again representing the spectral quantities as N-vectors composed of uniformly-spaced samples and approximating the integral by a summation, the scanner model in (12) can be compactly written in matrix-vector notation as

$$\mathbf{t} = \mathbf{M}^T\mathbf{r} \tag{13}$$

where $\mathbf{t} = [t_1, t_2, t_3]^T$ is the vector of scanner RGB responses, $\mathbf{r}$ is the $N \times 1$ vector of reflectance samples, $\mathbf{M}$ is an $N \times 3$ matrix whose i^{th} column $\mathbf{m}_i$ is the spectral sensitivity of the i^{th} channel, and the superscript T denotes the transpose operation.

3.3. Model-based Scanner Calibration

The idea behind model-based scanner calibration is to exploit models for the medium and the scanner to obtain a calibration transformation. The RGB values obtained from the scanner provide information regarding the reflectance spectrum of the pixel scanned. This information is, however, of an incomplete nature because many different (in fact, and infinite number) reflectance N-vectors can result in the same output triplet of scanner RGB values. The scanner model of (13) provides a means for better describing the information provided by the scanner RGB values regarding the reflectance spectrum of the input. The reflectance spectrum for a pixel with scanner RGB values given by the vector $\mathbf{t}$ must lie in the set of all possible reflectances that produce the given scanner response $\mathbf{t}$. Using the model of (13), this set of all possible reflectances that produce the scanner response $\mathbf{t}$ is mathematically defined as

$$S^{scn}(\mathbf{t}) = \{\mathbf{r} \mid \mathbf{M}^T\mathbf{r} = \mathbf{t}\} \tag{14}$$

If it is also known that the scanned medium corresponds to the model presented in(8), the input reflectance lies in the set S^{med} of reflectances producible on the medium defined in (11). Combining the information provided by the scanner RGB values and the scanner model with that for the medium, one can deduce that the reflectance spectrum of the scanned pixel lies in the intersection $S^{med} \bigcap S^{scn}(\mathbf{t})$ of the sets predicated by the scanner model and the model for the medium. For a single photographic medium and typical scanner sensitivities, it is unlikely that "scanner metamers", i.e., different reflectance spectra that appear identical to the scanner will be encountered[‖]. Therefore, the intersection represents a singleton (one-element) set.

From the above description, it is clear that the input reflectance reflectance spectrum can be estimated if an algorithm is available for obtaining a reflectance in the intersection of the sets S_0^{med} and $S^{scn}(\mathbf{t})$. Set-theoretic estimation methods [5] specifically address the problem of determining an element in the intersection of a number of constraint sets. The most powerful and useful set-theoretic estimation algorithms are variants of the method of successive projections onto convex sets (POCS) [5], which determines an element lying in the intersection of a number of closed-convex sets by starting with an arbitrary point and successively projecting onto the sets till convergence is achieved.

The set $S^{scn}(\mathbf{t})$ is a closed convex set (under the normal Hilbert space [22] structure on $\mathbb{R}^N$) but the set S_0^{med} is not a convex set (in the same Hilbert space). Therefore, the POCS method cannot be directly applied to the model-based scanner calibration problem. Note, however, that the set S_0^{med} is closed and convex in the density domain. The problem can therefore be formulated in the generalized product space framework proposed recently in [23]. By introducing a suitable Hilbert space structure over the space of reflectance spectra which makes the set S_0^{med} convex, the POCS algorithm can be used. We summarize only the results using the algorithm here and refer the reader to [8] for theoretical details and to [9] for details of the practical implementation of the method.

The model-based scanner calibration method was tested using the Kodak IT8 photographic target [17]. The reflectance spectra for the 264 patches in the Kodak IT8 target were measured independently using a spectrophotometer. The reflectance of the white patch in the gray-wedge on the target is used as the reflectance of the paper substrate $\mathbf{r}_p$ in computing paper-relative spectral densities. The first three principal components of the 264 densities account for 97.2% of the signal energy in density space, and are used as the (orthonormal) densities $\mathbf{o}_1, \mathbf{o}_2, \mathbf{o}_3$ of three principal dyes in the media model of (11).

A three channel UMAX color scanner was used for experimental evaluation of the technique. Since the scanner spectral sensitivity matrix M was not directly available, these was first estimated by the principal eigenvector technique described in [24] to obtain the scanner model of (14). The scanner was used to acquire an RGB image of the Kodak IT8 target and the average RGB value corresponding to each of the color patches on the target was computed. These scanner RGB values were used along with the scanner and media models in the model-based calibration method outlined earlier.

Figure 5 illustrates some of the typical results obtained from this procedure. The solid lines in the figure represent the actual measured reflectances corresponding to Kodak IT8 patches and the broken line closest to

[‖]In the presence of "scanner metamers", the notion of what constitutes a valid scanner calibration itself becomes debatable.

each of the solid lines represents the corresponding estimate obtained by the model-based calibration procedure. From the plots, once can see that the the errors in the spectral estimates are quite small.

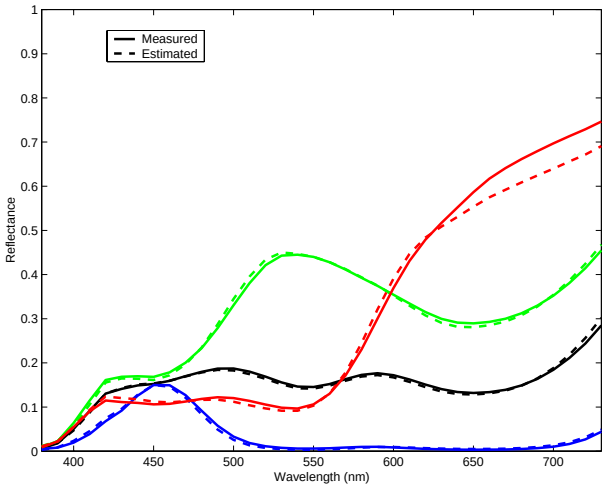

Figure 5. Representative results for the UMAX scanner calibration.

In order to quantify the accuracy of the model-based calibration scheme, the computed spectrum $\hat{\mathbf{r}}$ is compared with the actual spectrum $\mathbf{r}$ using three different metrics: 1) the normalized mean squared spectral error (NMSSE) defined (in dB) as

$$\text{MSE}_{spec} = 10 \log_{10} \left(\frac{\text{E}\{\| \mathbf{r} - \hat{\mathbf{r}} \|^2\}}{\text{E}\{\| \mathbf{r} \|^2\}} \right), \tag{15}$$

where $\text{E}\{\cdot\}$ denotes the average over the spectral ensemble (in this case the Kodak IT8 target spectra), 2) the ΔE^*_{ab} color-difference [25] under CIE D50 daylight illuminant, and 3) the ΔE^*_{94} color-difference [26] under CIE D50 daylight illuminant. The NMSSE measures the spectral error in the calibration and the ΔE metrics attempt to quantify the visual impact of the spectral errors.

For the model-based calibration for the UMAX scanner, over the Kodak IT8 target, the NMSSE was -31.03 dB and the average and maximum ΔE^*_{ab} errors were 1.76 and 7.15, respectively. The average and maximum values for the ΔE^*_{94} metric were 1.11 and 5.70, respectively. The low values of the errors illustrate that the model based technique provides an accurate spectral calibration of the scanner.

The model-based scanner calibration scheme presented in this section once again integrates physical modeling with appropriate mathematical tools of linear algebra and set theoretic estimation to provide a novel solution to the problem of scanner calibration. The broader framework of the models and the underlying mathematical algorithms can also successfully address additional problems in the design of color filters and colorant formulation [8].

4. DISCUSSION AND SUMMARY

For both the case studies presented here, solutions to problems in imaging systems were determined using suitable physical models and mathematical tools. It is worth pointing out that the synergy and combination of these elements is what allows the solution and either one by itself is insufficient. For instance, in the case of show-through correction, the use of the gradient descent based LMS adaptive filtering by itself does not enable the solution, instead, the physical analysis that allows linearization of the problem is also a key element. In particular, the problem becomes linear when image data on the front side is converted to density and on the back side to absorptance, which is a rather non-intuitive result and could be inferred only through the use of the physical model. Vice-versa, the physical modeling by itself is also rather simplistic and is not sufficient for solving

the problem since it does not readily allow us to compute the unknown show-through point-spread function or the alignment between the images on the two sides.

The two examples presented demonstrate how a blend of physical modeling with mathematical tools can produce powerful solutions for problems in imaging systems. This is a particularly common and powerful motif in imaging systems research that is supported by numerous other examples including several additional ones from our own work on estimation of device spectral sensitivities [24], quality measures for color recording devices [27], and show-through watermarking [28]. The interdisciplinary nature of work in imaging systems makes these approaches that combine physics and mathematics harmoniously even more compelling than other areas of research.

REFERENCES

1. A. V. Oppenheim, A. S. Willsky, and S. H. Nawab, *Discrete Time Signal Processing*, Prentice-Hall, Englewood Cliffs, N.J., second ed., 1997.
2. A. V. Oppenheim and R. W. Schafer, *Discrete Time Signal Processing*, Prentice-Hall, Englewood Cliffs, N.J., second ed., 1992.
3. J. S. Lim, *Two Dimensional Signal and Image Processing*, Prentice Hall, Englewood Cliffs, NJ, 1990.
4. J. M. Wozencraft and I. Jacobs, *Principles of Communication Engineering*, John Wiley and Sons, New York, 1965.
5. P. L. Combettes, "The foundations of set theoretic estimation," *Proc. IEEE* **81**, pp. 182–208, Feb. 1993.
6. S. Haykin, "Signal processing: where physics and mathematics meet," *IEEE Sig. Proc. Mag.* **18**, pp. 6–7, Jul. 2001.
7. G. Sharma, "Show-through cancellation in scans of duplex printed documents," *IEEE Trans. Image Proc.* **10**, pp. 736–754, May 2001.
8. G. Sharma, "Set theoretic estimation for problems in subtractive color," *Color Res. Appl.* **25**, pp. 333–348, October 2000.
9. G. Sharma, "Target-less scanner color calibration," *J. Imaging Sci. and Tech.* **44**, pp. 301–307, Jul./Aug. 2000.
10. S. Haykin, *Adaptive Filter Theory*, Prentice Hall, NJ, fourth ed., 2002.
11. B. K. P. Horn, "Exact reproduction of color images," *Comp. Vis., Graphics and Image Proc.* **26**, pp. 135–167, 1984.
12. H. J. Trussell and J. R. Sullivan, "A vector-space approach to color imaging systems," in *Proc. SPIE: Image processing algorithms and techniques*, K. S. Pennington, ed., **1244**, pp. 264–271, Feb. 1990.
13. H. J. Trussell, "DSP solutions run the gamut for color systems," *IEEE Sig. Proc. Mag.* **10**, pp. 8–23, Apr. 1993.
14. G. Sharma and H. J. Trussell, "Digital color imaging," *IEEE Trans. Image Proc.* **6**, pp. 901–932, Jul. 1997.
15. H. J. Trussell, "Application of set theoretic models to color systems," *Color Res. Appl.* **16**, pp. 31–41, Feb. 1991.
16. Y. Yang and H. Stark, "Solutions of several color-matching problems using projection theory," *J. Opt. Soc. Am. A* **11**, pp. 89–96, Jan. 1994.
17. M. Nier and M. E. Courtot, eds., *Standards for electronic imaging systems : proceedings of a conference held 28 Feb.-1 March 1991, San Jose, California*, vol. CR37 of *Critical reviews of optical science and technology*, SPIE, Bellingham, WA, 1991.
18. F. Grum and C. J. Bartleson, eds., *Optical Radiation Measurements: Color Measurement*, vol. 2, Academic Press, New York, 1983.
19. I. T. Jolliffe, *Principal Components Analysis*, Springer-Verlag, Berlin, 1986.
20. J. A. S. Viggiano and C. J. Wang, "A novel method for colorimetric calibration of color digitizing scanners," *TAGA Proceedings* , pp. 143–160, 1993.
21. R. S. Berns and M. J. Shyu, "Colorimetric characterization of a desktop drum scanner using a spectral model," *J. Electronic Imaging* **4**, pp. 360–372, Oct. 1995.
22. A. Friedman, *The Foundations of Modern Analysis*, Dover, New York, 1982.

23. P. L. Combettes, "Generalized convex set theoretic image recovery," in *Proc. IEEE Intl. Conf. Image Proc.*, **II**, pp. 453–456, Sept. 1996.
24. G. Sharma and H. J. Trussell, "Set theoretic estimation in color scanner characterization," *J. Electronic Imaging* **5**, pp. 479–489, Oct. 1996.
25. CIE, "Colorimetry." CIE Publication No. 15.2, Central Bureau of the CIE, Vienna, 1986. The commonly used data on color matching functions is available at the CIE web site at http://www.cie.co.at/.
26. CIE, "Industrial color difference evaluation." CIE Publication No. 116-1995, Central Bureau of the CIE, Vienna, 1995.
27. G. Sharma and H. J. Trussell, "Figures of merit for color scanners," *IEEE Trans. Image Proc.* **6**, pp. 990–1001, Jul. 1997.
28. G. Sharma and S. Wang, "Show-through watermarking of duplex printed documents," in *Proc. SPIE: Security, Steganography, and Watermarking of Multimedia Contents VI*, E. J. Delp and P. W. Wong, eds., **5306**, Jan. 2004.